## SUPPLEMENTAL FIGURE LEGENDS

**Figure S1. (A)** Confocal microscopy images of human BC tumor sections TEM showing that in BC, $CD14^+$ expressing TIE-2 (i.e. TEM) are $CD45^+$, $CD11c^-$ and $HLA\text{-}DR^+$. Scale bar: 25 µm; **(B)** Gating strategy for the identification of TEM by flow cytometry. Profiles of dissociated breast carcinoma stained for CD11b, CD14, TIE-2 and VEGFR-1 (please see also supplemental information online of [26]). One representative example out of ten is shown.

**Figure S2: TEM express VEGFR-1. (A)** High magnification confocal microscopy images of TEM showing expression of VEGFR-1; **(B)** Confocal microscopy images of negative and positive controls: immunohistochemical stainings in frozen sections of BC; **(C)** HE and enzymatic staining for CD14. Scale bars: 5 µm (A), 50 µm (B) and 100 µm (C).

**Figure S3: TEM characterization in BC sections. (A)** Spearman's rank correlation coefficient ($\rho$) determination. The correlation between VEGFR-1 and TIE-2 expression levels was used as a positive control. Representative confocal image for TIE-2 immunofluorescence signal with a display of the tiles used for quantification (in green, left panel); corresponding dot plot representing VEGFR-1 versus TIE-2 signal for individual tiles (middle panel). Spearman's rank correlation coefficient is calculated for tiles retained after applying a threshold in both channels (excluded tiles are in red); VEGFR-1 and TIE-2 expression levels show a robust correlation ($\rho$ = 0.90 ± 0.05, 7 patients) in images from BC tumor sections (right panel); **(B)** Representative dot plots for the absence of correlation between CD14 and CD31 expression levels: the negative control (left panel, no primary antibody) shows that a threshold at $10^4$ in both channels removes 99.98% of the background signal; Representative example where CD14 and CD31 expression levels exhibited no correlation (middle panel). 16% of the CD14 tiles are above the threshold. 18% of CD31 tiles are above the threshold. However, only 1.5% of the $CD14^+$ tiles were $CD31^+$ tiles (representing 1.7% of the total CD31 signal in $CD14^+$ tiles) which reflect an absence of

correlation ($\rho$ = 0.055); Example of image with artifactually high Spearman's rank correlation coefficient ($\rho$ = 0.751) (right panel). In this case, 49% of the $CD14^+$ tiles were between the two thresholds. 24% of $CD31^+$ tiles were between the two thresholds (saturating CD31 signals were excluded from the analysis). Only 4.0% of the accepted $CD14^+$ tiles were $CD31^+$ tiles (7.7% of the total CD31 signal intensity in $CD14^+$ tiles) which means that the high correlation ($\rho$ = 0.751) applies only to a minority (7.7%) of $CD14^+$ tiles; **(C)** Representative confocal microscopy images of CD14 staining in tumor center, tumor invasive edge and peri-tumoral area (CD14 and CD3). These tumor zones are outlined on the corresponding HE staining. T cell-TEM conjugates were observed at the limit or the peri-tumoral zone as we previously reported.[27] Scale bars: 25 µm (fluorescence) and 200 µm (HE); **(D)** Correlation between TEM angiogenic activity - as measured with our algorithm on BC sections and defined as the product of the percentage of the tumor area covered by CD14 cells × the mean fluorescence intensity of CD14- and the lymphocyte infiltrate, quantified according to the guidelines of Saldago.[35] TEM angiogenic activity correlates with the ratio of CD14 to lymphocyte infiltrate. Breast cancer subtypes and raw data are indicated in the table below the graph. By contrast, TEM angiogenic activity did not correlate with lymphocyte infiltrate.

**Figure S4. TEM co-express LEC markers.** High magnification confocal microscopy images of TEM showing co-expression of the canonical LEC markers VEGFR-3, Podoplanin and LYVE-1 and PROX-1. Scale bar: 5 µm.

**Figure S5: Clustered TEM express lymphatic markers in BC tumors. (A)** In these structures, TEM were PROX-$1^+$ and Podoplanin$^+$ as well as LYVE-$1^+$ (Fig. 3C). Scale bar: 25 µm; **(B)** In clusters of TEM, CD14 expression was correlated with the expression of Podoplanin ($\rho$ = 0.879, left panel), PROX-1 ($\rho$ = 0.845, middle panel) and LYVE-1 ($\rho$ = 0.786, data not shown). Consequently, Podoplanin and PROX-1 show a high Spearman's rank correlation coefficient as well ($\rho$ = 0.882, right panel).

**Figure S6: TEM were found associated with lymphatic structures in human breast tumor tissues. (A)** Representative example of tumor lymphatics containing TEM ($CD14^+Podoplanin^+TIE\text{-}2^+$ cells); **(B)** TEM associated with these structures also expressed LYVE-1 and PROX-1, confirming a phenotype overlapping with LEC; **(C)** In contrast, immunofluorescence labelling in sections of non-neoplastic breast tissue adjacent to tumor tissues show no TEM association with lymphatic vessels ($Podoplanin^+$). Scale bars (A-C): 25 µm.

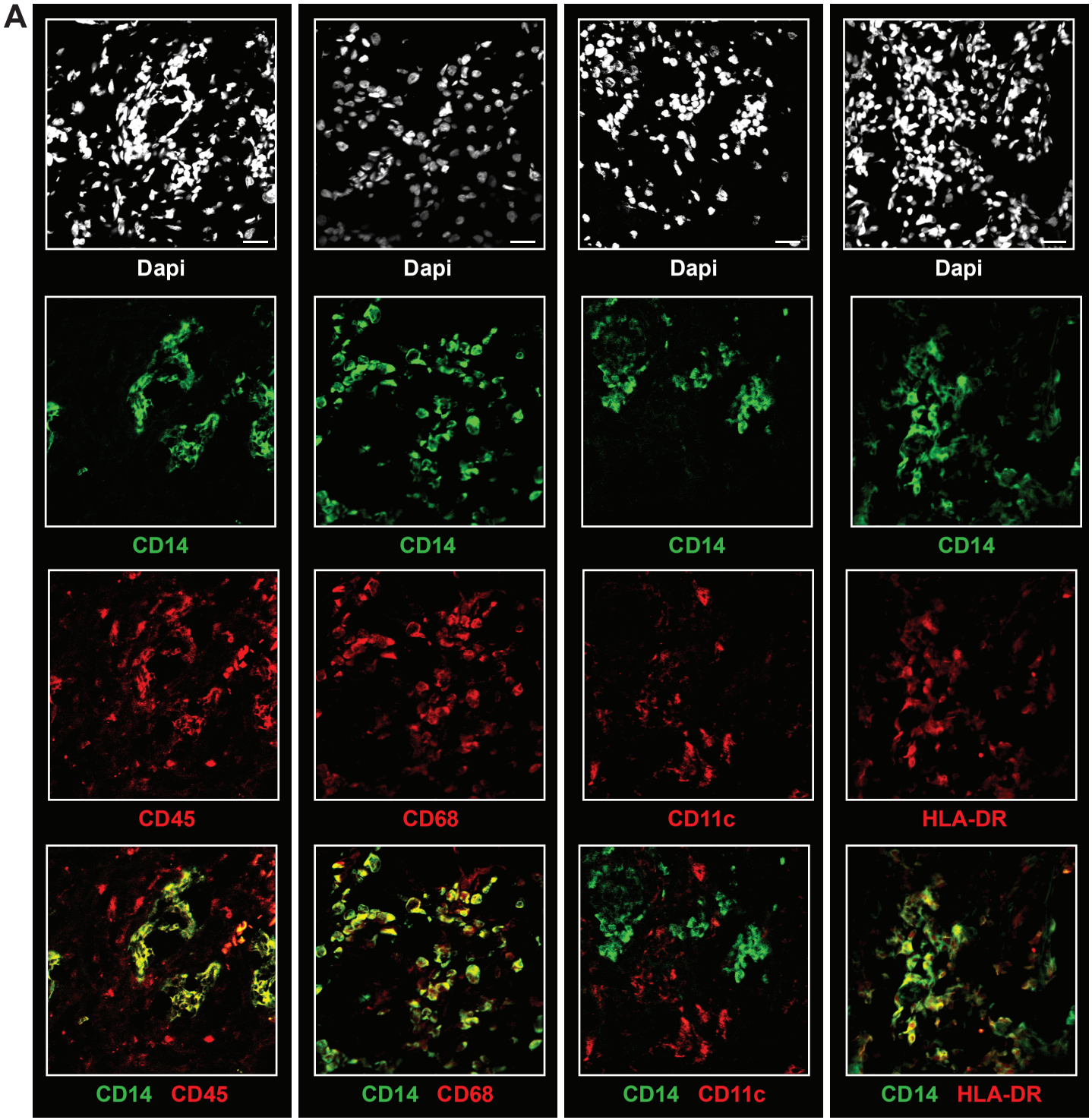
A
Dapi
Dapi
Dapi
Dapi
CD14
CD14
CD14
CD14
CD45
CD68
CD11c
HLA-DR
CD14 CD45
CD14 CD68
CD14 CD11c
CD14 HLA-DR

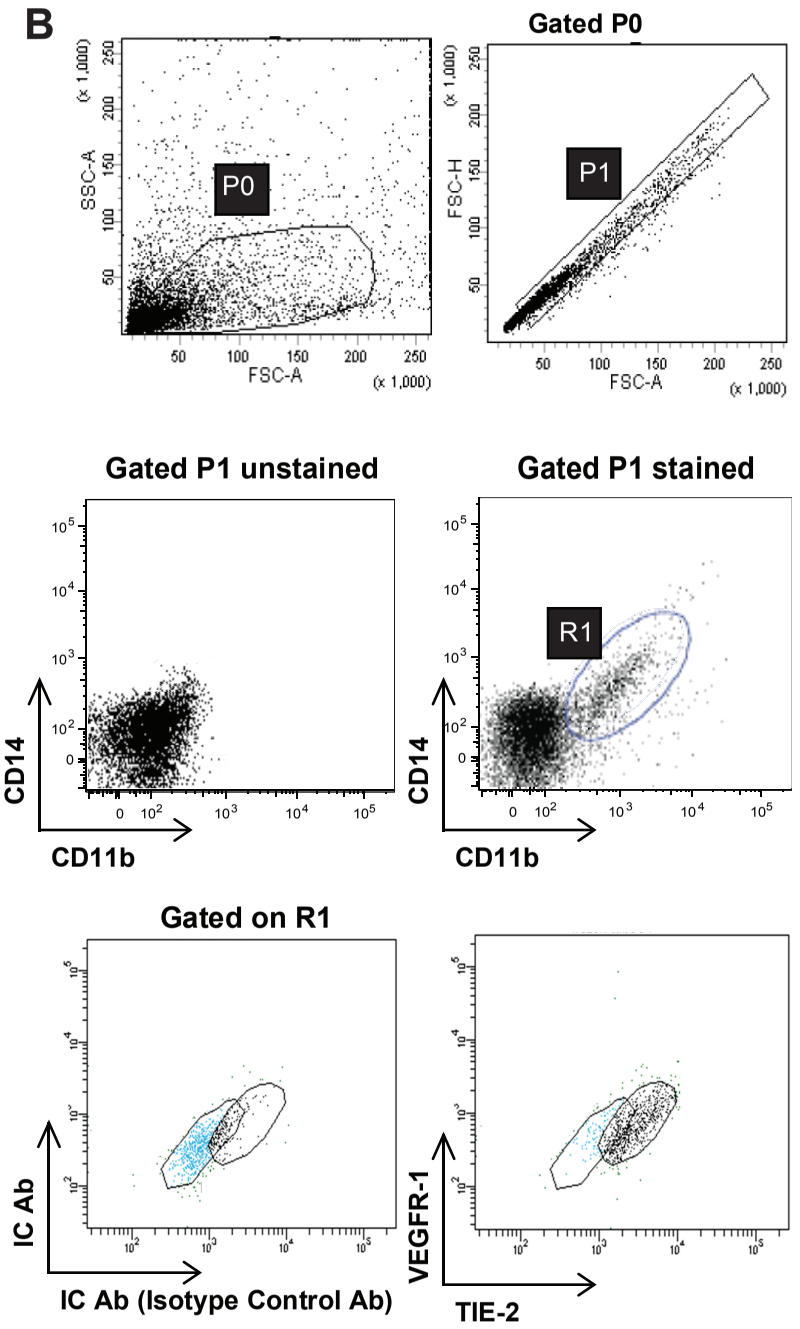
B
Gated P0
SSC-A
FSC-A
P0
FSC-H
FSC-A
P1
Gated P1 unstained
Gated P1 stained
CD14
CD11b
R1
Gated on R1
IC Ab
IC Ab (Isotype Control Ab)
VEGFR-1
TIE-2

Figure S1

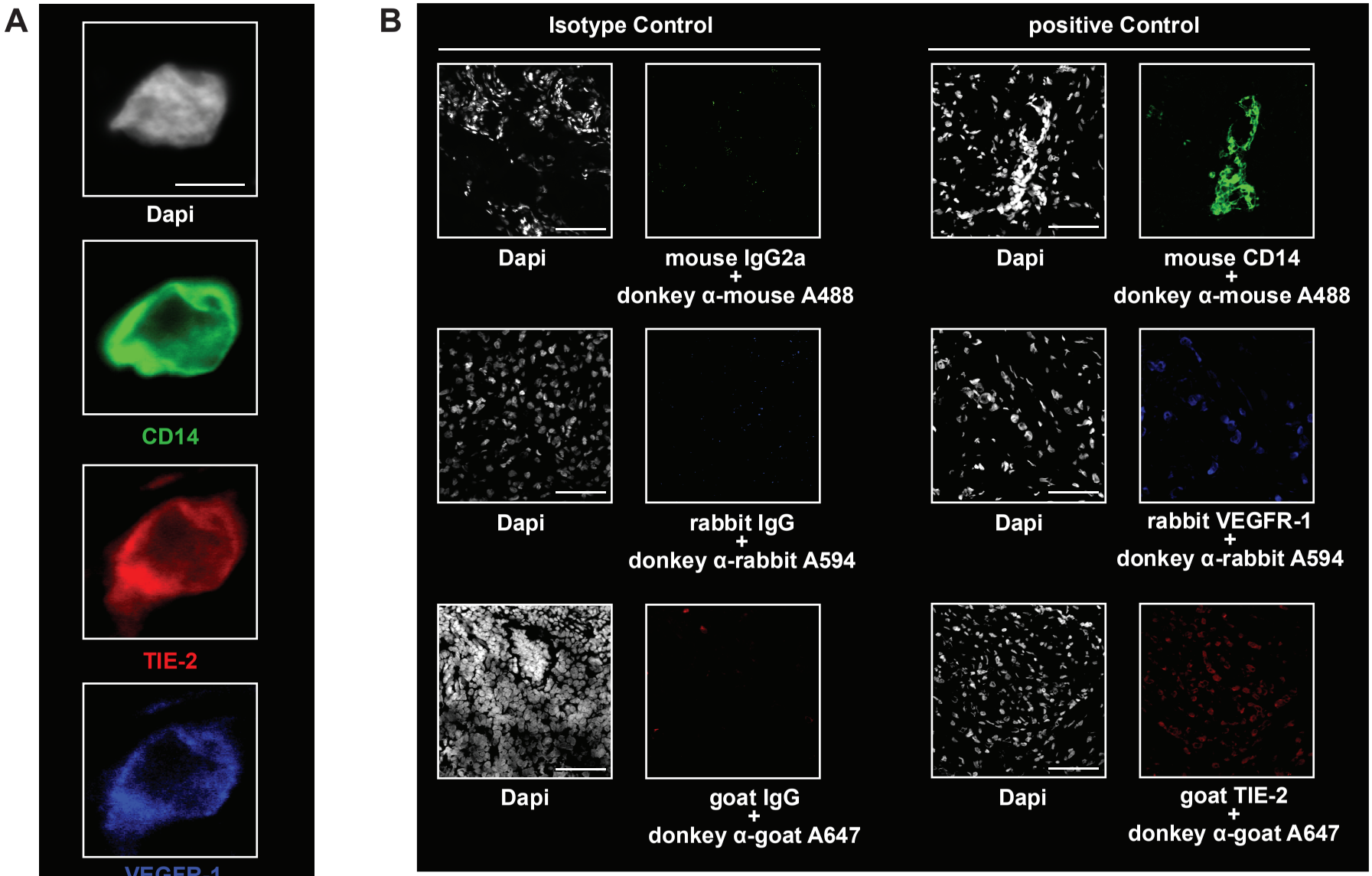
A
Dapi
CD14
TIE-2
VEGFR-1
CD14 TIE-2 VEGFR-1
B
Isotype Control
positive Control
Dapi
mouse IgG2a
+
donkey α-mouse A488
Dapi
mouse CD14
+
donkey α-mouse A488
Dapi
rabbit IgG
+
donkey α-rabbit A594
Dapi
rabbit VEGFR-1
+
donkey α-rabbit A594
Dapi
goat IgG
+
donkey α-goat A647
Dapi
goat TIE-2
+
donkey α-goat A647

Figure S2

C

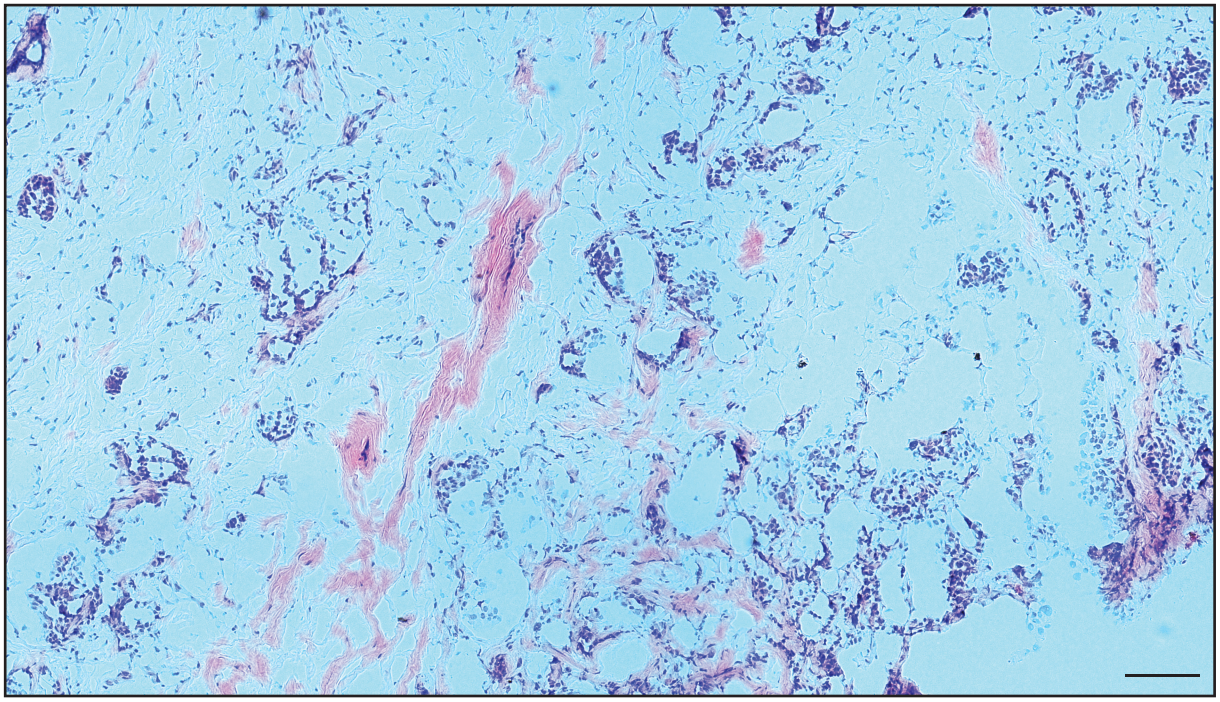

HE

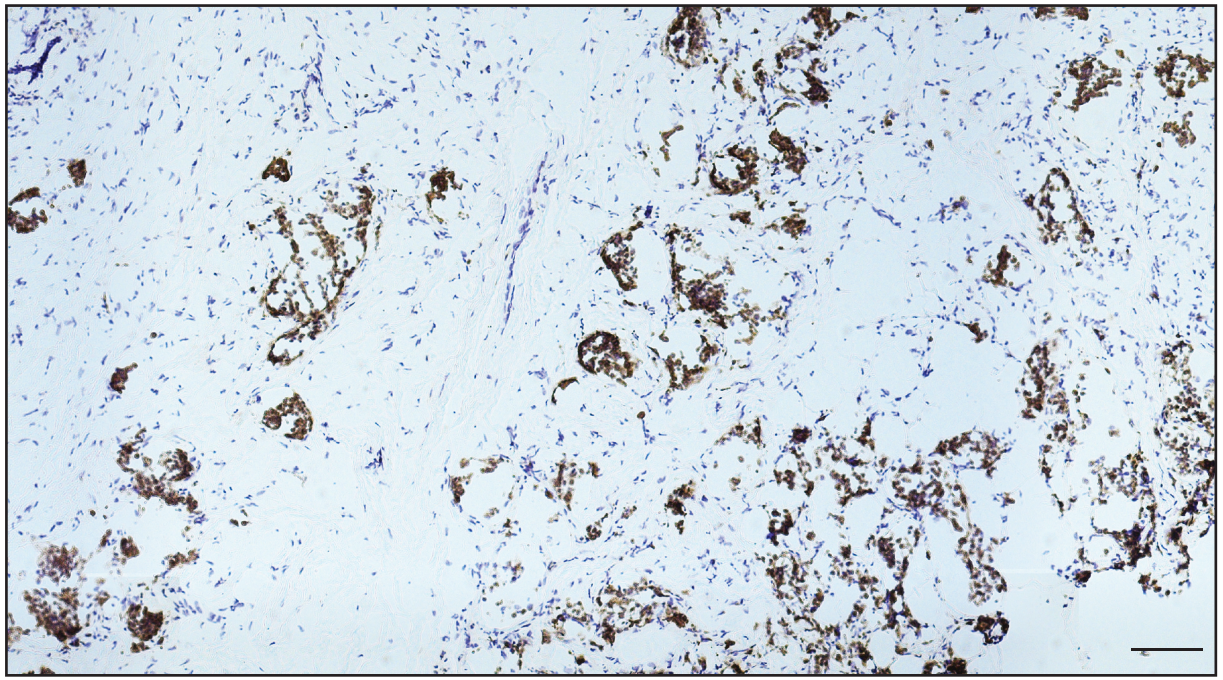

enzymatic CD14

Figure S2

A

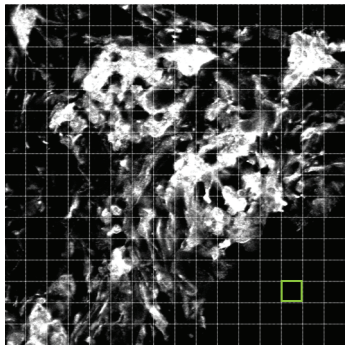

Virtual image for TIE-2

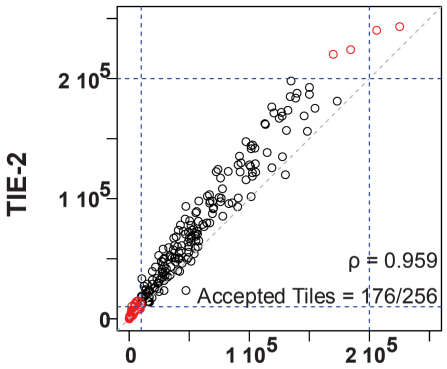


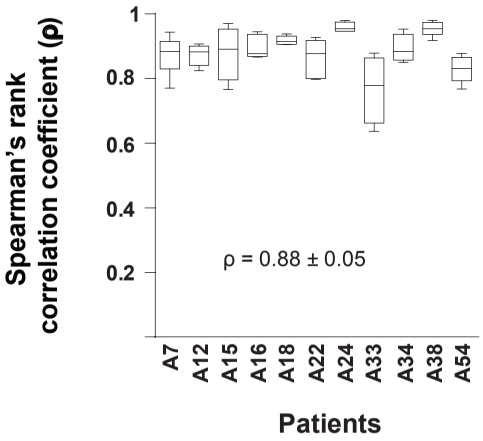


B

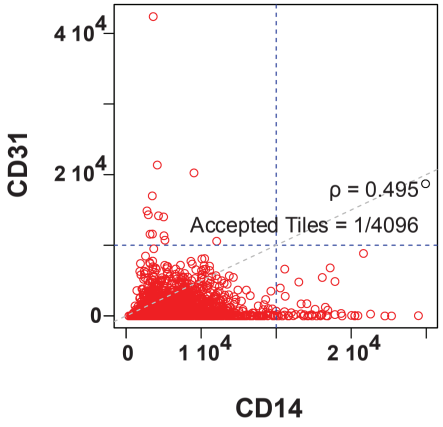


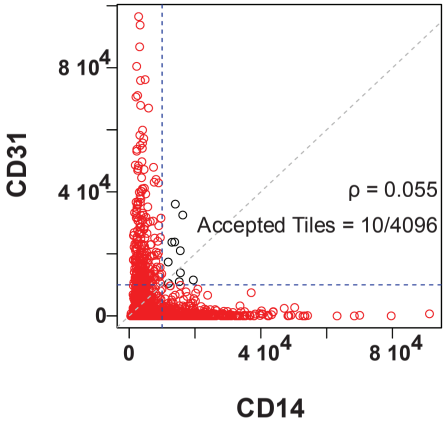


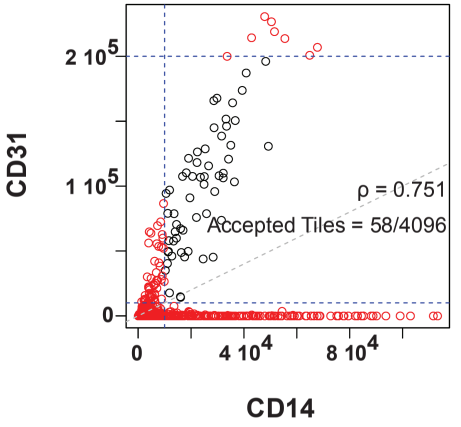


Figure S3

C

Tumor center

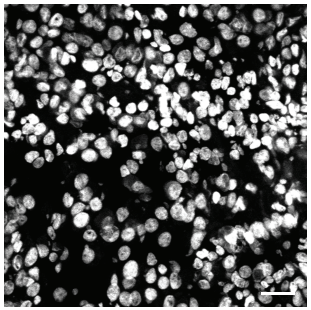

Dapi

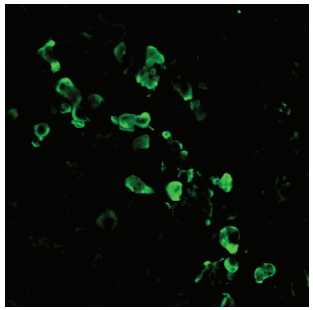

CD14

Tumor invasive edge

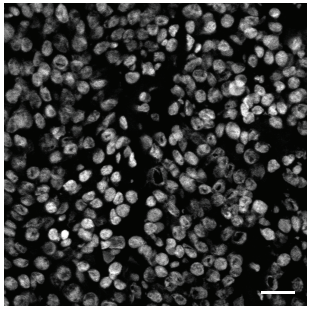

Dapi

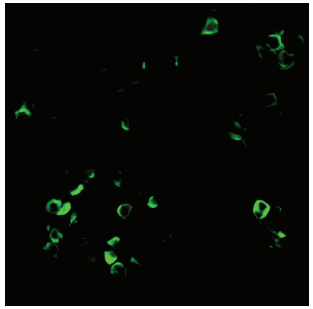

CD14

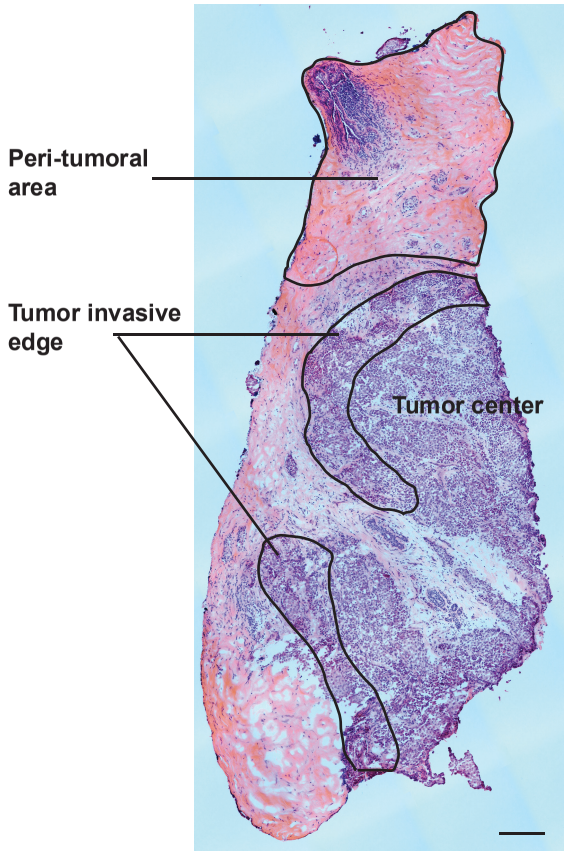


Peri-tumoral area

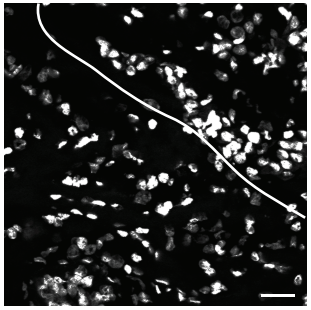

Dapi

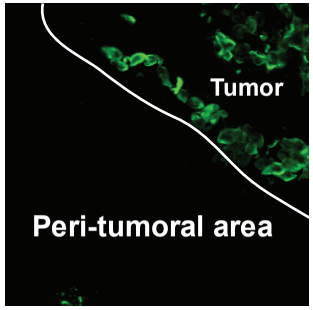


CD14

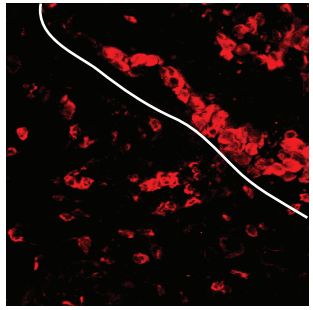

CD3

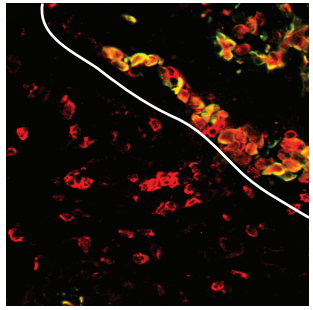

CD14 CD3

D

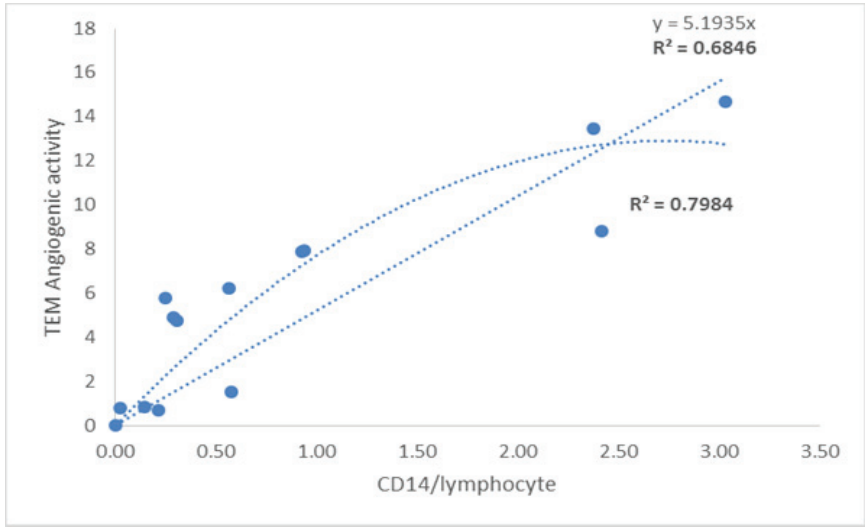


| BC subtype | % lymphocyte infiltrate | CD14/lympho |
|---|---|---|
| Luminal A, grade II | 5 | 0.216 |
| Luminal B, grade II | 7 | 0.003 |
| Luminal B, grade III | 17 | 0.929 |
| Luminal B, grade III | 35 | 0.251 |
| Triple negative, grade III | 40 | 0.026 |
| Luminal B, grade I | 6 | 0.575 |
| Luminal A, grade I | 15 | 3.033 |
| Luminal B, grade II | 20 | 0.290 |
| Luminal A, grade I | 20 | 0.305 |
| Luminal A, grade II | 12 | 2.417 |
| Luminal B, grade III | 27 | 0.941 |
| Luminal B, grade II | 4 | 2.375 |
| Luminal A, grade III | 17 | 0.147 |
| Luminal A, grade II | 22 | 0.564 |

**Figure S3**

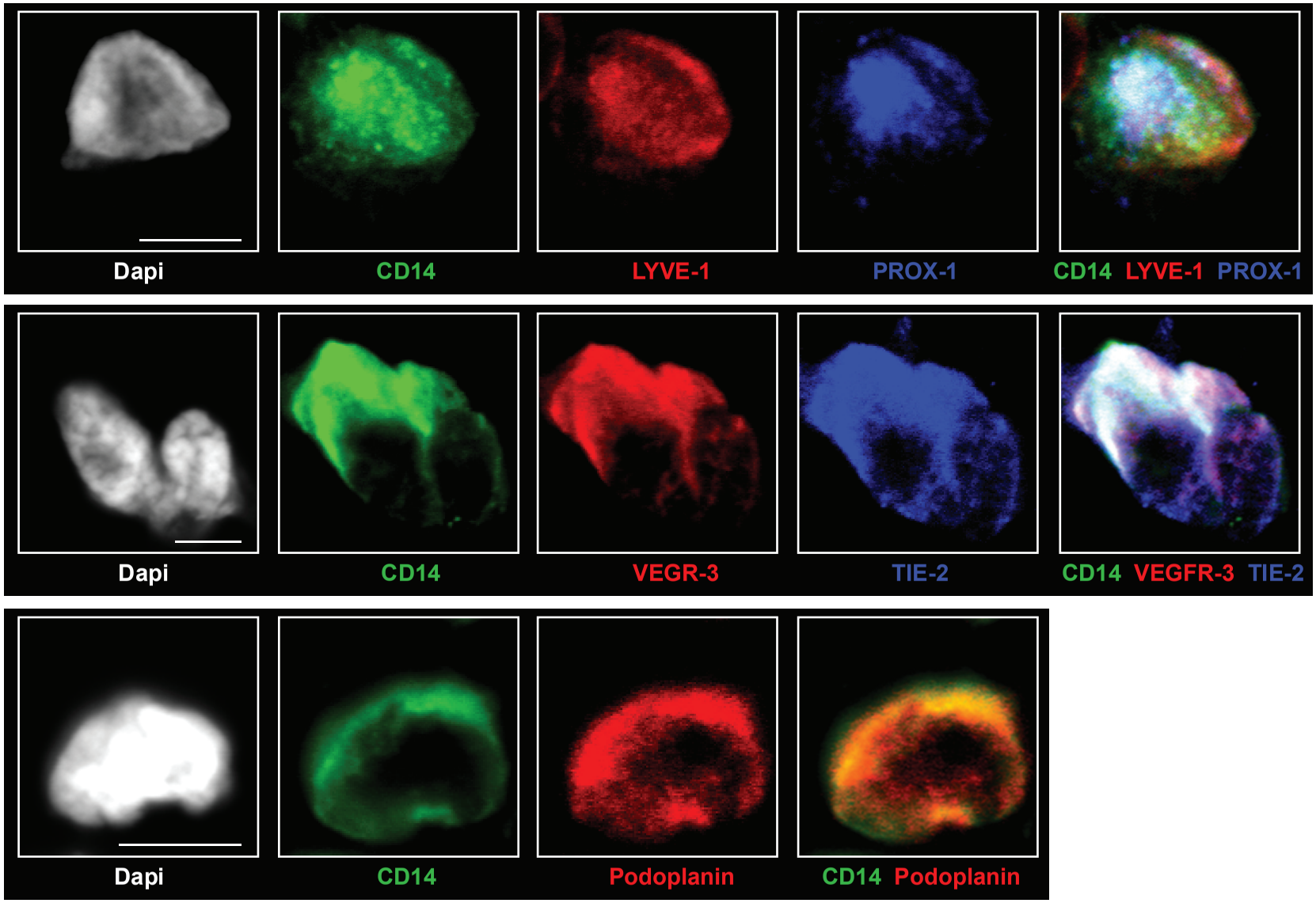
Dapi
CD14
LYVE-1
PROX-1
CD14 LYVE-1 PROX-1
Dapi
CD14
VEGR-3
TIE-2
CD14 VEGFR-3 TIE-2
Dapi
CD14
Podoplanin
CD14 Podoplanin

**Figure S4**

A

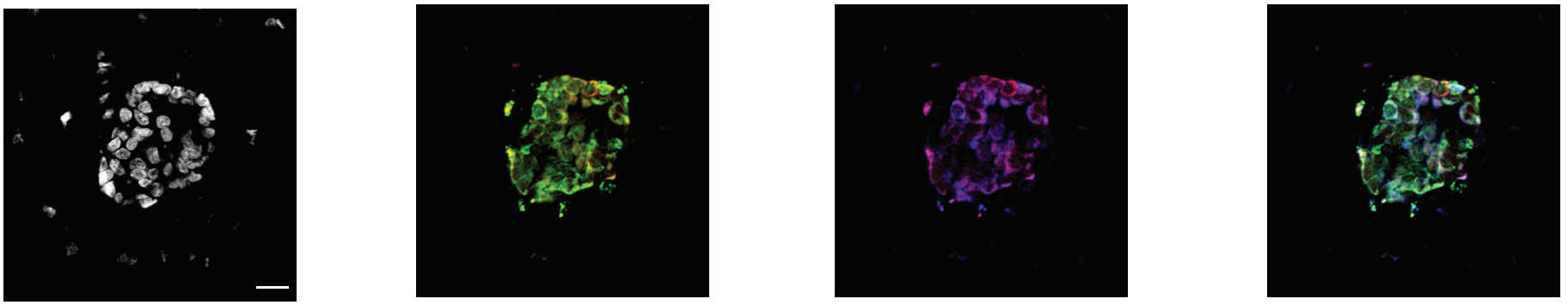
Dapi
CD14 Podoplanin
Podoplanin PROX-1
CD14 Podoplanin PROX-1

B

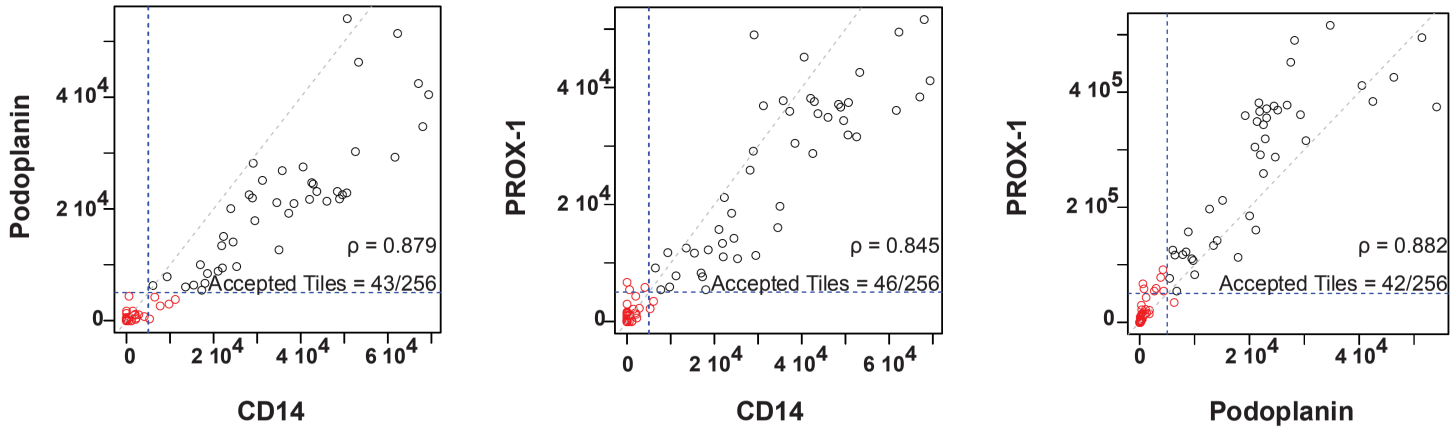
Podoplanin
4 10^4
2 10^4
0
ρ = 0.879
Accepted Tiles = 43/256
0
2 10^4
4 10^4
6 10^4
CD14
PROX-1
4 10^4
2 10^4
0
ρ = 0.845
Accepted Tiles = 46/256
0
2 10^4
4 10^4
6 10^4
CD14
PROX-1
4 10^5
2 10^5
0
ρ = 0.882
Accepted Tiles = 42/256
0
2 10^4
4 10^4
Podoplanin

Figure S5

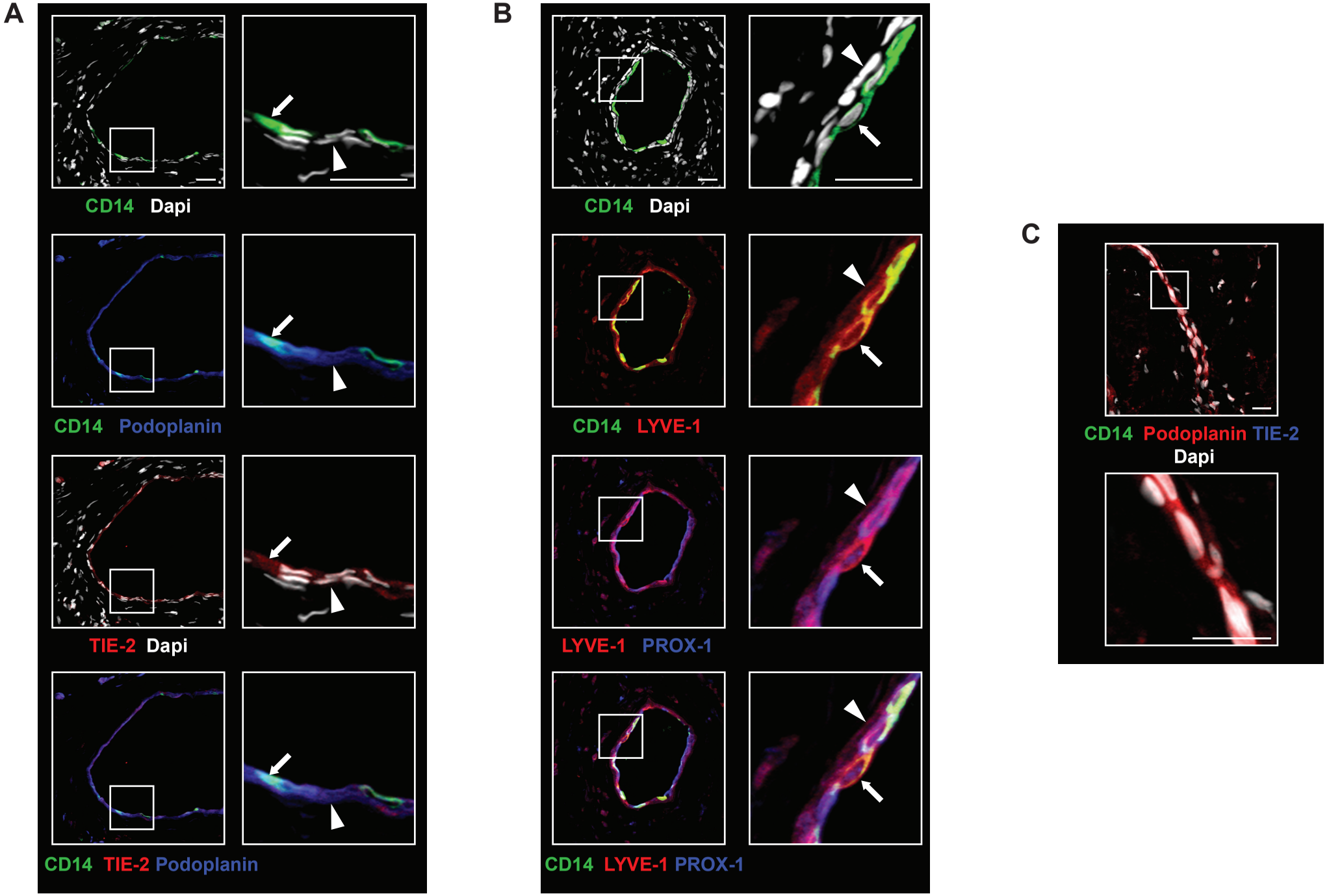
A
CD14 Dapi
CD14 Podoplanin
TIE-2 Dapi
CD14 TIE-2 Podoplanin
B
CD14 Dapi
CD14 LYVE-1
LYVE-1 PROX-1
CD14 LYVE-1 PROX-1
C
CD14 Podoplanin TIE-2
Dapi

Figure S6